

## Enhancing the Anticancer Activity of Squamocin for Breast Cancer Treatment Using Nanodiamond Nanoparticles: An *In Vivo* Study

Firli Rahmah Primula Dewi<sup>1\*</sup>, Sri Puji Astuti Wahyuningsih<sup>1</sup>, Rasyidah Fauzia Ahmar<sup>1</sup>, Na'ilah Insani Alifiyah<sup>1</sup>, Vuanghao Lim<sup>2</sup>, Muhammad Darwin Prenggono<sup>3</sup>

<sup>1</sup>Department of Biology, Faculty of Science and Technology, Universitas Airlangga, Surabaya, Indonesia

<sup>2</sup>Advanced Medical and Dental Institute, Universiti Sains Malaysia, Penang, Malaysia

<sup>3</sup>Division of Hematology, Medical Oncology, Ulin General Hospital, Banjarmasin, Indonesia

### ARTICLE INFO

#### Article history:

Received April 29, 2022

Received in revised form July 28, 2022

Accepted August 1, 2022

#### KEYWORDS:

Breast cancer,  
drug delivery,  
nanodiamond,  
NMU,  
squamocin

### ABSTRACT

Squamocin is one of the annonaceous acetogenins produced by the Annonaceae family and displays potent anti-cancer activity against cancer cell lines. This study aimed to investigate the growth inhibition activity of squamocin coupled with nanodiamond on rats (*Rattus norvegicus*)-induced breast cancer. Twenty-five female *R. norvegicus* were divided into five groups (n = 5), including normal control (without any treatment), negative control, group treated with nanodiamond only (ND), group treated with squamocin only (SQ), and the group treated with squamocin coupled with nanodiamond (NDSQ). All of the animal models were induced for breast cancer, except for the normal control group. Breast cancer induction was performed using two doses of N-nitroso-N-methylurea (NMU) injection (50 and 30 mg/kg body weight) intraperitoneally and waited for 22 weeks until the tumor was detected to formed. Nanodiamond coupled with squamocin were administered by intraperitoneal injection (1.5 mg/kg body weight) for 5 weeks, one injection per 3 days. This study showed that the treatment with squamocin coupled with nanodiamond (NDSQ) significantly reduced the proliferation (Ki-67) and induced apoptosis (Caspase-3) of breast cancer cells, corresponding to the reduction of the thickness of the mammary ductal epithelium (p<0.001) and the lower level of CA-153 in serum. In addition, the treatment significantly reduced the malondialdehyde (MDA) and PI3KCA and increased the p53 level significantly. Altogether, in this study, we are the first to report the anti-cancer activity of squamocin in rat-induced breast cancer and the potency of nanodiamond as a carrier of squamocin to increase its anti-cancer activity.

## 1. Introduction

Breast cancer is one of the most common cancers among women and one of the leading causes of death worldwide. In 2020, there were 2.3 million women diagnosed with breast cancer and 685,000 deaths globally. As of the end of 2020, there were 7.8 million women alive diagnosed with breast cancer in the past 5 years, making it the world's most prevalent cancer (Velazquez *et al.* 2018). Due to the complexity of the tumor microenvironment, developing effective anti-cancer therapies remains challenging (Balkwill *et al.* 2012). The tumor microenvironment supports tumor progression, drives therapeutic response or

resistance, and creates immunological tolerance (Li and Burgess 2020).

Targeting oncogenic factors in the tumor microenvironment are the most common strategy for cancer treatment (Balkwill *et al.* 2012; Bahrami and Hassanian 2018; Cheng *et al.* 2016). Conventional drug delivery systems may fail to deliver an adequate quantity of therapeutic agents to kill cancer cells effectively without side effects due to the complexity of the tumor microenvironment. Drug targeting strategies, including nanoparticle-based drug delivery systems, are being studied to increase therapeutic efficiency (Danhier 2016; Ghaferi *et al.* 2022; Li *et al.* 2011). Among the delivery vehicle that is showing promising results are nanodiamond and nanotubes (Li and Burgess 2020). Nanodiamonds are promising results in serving the purpose due to high

\* Corresponding Author

E-mail Address: firli.rahmah@fst.unair.ac.id

colloidal stability in both aqueous and non-aqueous media (Purtov *et al.* 2010).

The phosphatidyl inositol 3 kinase (PI3K) pathway is a complicated intracellular network that plays an essential role in breast cancer cell growth and proliferation. The most important role in this pathway is regulated by the PI3K heterodimer, which belongs to the class IA of PI3Ks (Paplomata and O'Regan 2014). Multiple compounds targeting this pathway are being evaluated in clinical trials. However, delivering an adequate amount of the drug compound remains challenging due to the complexity of the tumor microenvironment. Squamocin is an annonaceous acetogenin compound from the Annonaceae family. Several *in vitro* studies reported the cytotoxicity effect of squamocin against several cancer cell lines, including H460, BGC805, BEL7402, HepG2, and SMCC-7721 (Liaw *et al.* 2010; Lu *et al.* 2006; Miao *et al.* 2016).

There are promising results when nanodiamond is used as a carrier of drugs in cancers (Wei *et al.* 2019). Due to its biocompatibility property, nanodiamond has the potential to be used as a carrier to deliver squamocin to breast cancer microenvironments and enhance its bioavailability and activity. Despite the possibility, no *in vivo* studies have been conducted to investigate the possibility of using nanodiamond as a carrier of squamocin. Therefore, this study aims to investigate the growth inhibition activity of squamocin coupled with nanodiamond on rats (*Rattus norvegicus*)-induced breast cancer.

## 2. Materials and Methods

### 2.1. Ethics Approval

Animal Care and Use Committee approved all animal model experiments, Faculty of Animal Health, Universitas Airlangga, Surabaya, Indonesia (No. 2.KE.046.04.2021).

### 2.2. Animals

Twenty-five (25) female rats, species *Rattus norvegicus* (4-8 weeks old, 250-300 g), were placed in plastic cages covered by wire gauze. Five rats of each group were arranged as 1-2 rats/cage. The rats were kept in the conditions maintained in a 12 hrs/dark-light cycle and allowed free access to food and water during the experiments. Before the commencement of the treatments, the rats were acclimatised for two weeks.

### 2.3. Experimental Design

Rats were randomly divided into six groups (n = 5): (1) Normal control (NC), without any treatment;

(2) Negative control (K-), exposed with NMU without NDSQ administration; (3) Nanodiamond-treated (ND) group, exposed with NMU and injected with nanodiamond only; (4) Squamocin-treated (SQ) group, exposed with NMU and injected with 1.5 mg/kg body weight of squamocin only; (5) Squamocin coupled with nanodiamond-treated (NDSQ) group, exposed with NMU and injected with 1.5 mg/kg body weight of squamocin coupled with nanodiamond. Breast cancer was induced by injecting NMU intraperitoneally twice. The first NMU dose for injection was 50 mg/kg/body weight, and the second was 30 mg/kg/body weight. The breast cancer formation was assessed by palpitation, and when the breast cancer had formed, the rats were treated according to the respective group by intraperitoneal injection. The treatment was performed for five weeks, with one injection per 3 days. The concentration of squamocin (SQ) and squamocin coupled with nanodiamond for each injection was 1.5 mg/kg body weight. Squamocin was purchased from Anhui Minmetals Development LTD, China.

### 2.4. Conjugation of ND-Squamocin

The ND carboxyl-modified (1 mg/ml) with the molecules size average of 10 nm (TCI, N1084) was sonicated using a probe sonicator for 5 minutes. EDC (8.35 µg) and sulfo-NHS (9.5 µg) dissolved in water were then added to the ND suspension. After 30 minutes of stirring, 200 µg of mPEG-amine was added to the activated ND solution and stirred overnight at room temperature. The excess reagents were removed by centrifugation at 14,000 rpm for two hours, and the pellet was washed in deionised water. The pellet was dispersed in 2.5 mM NaOH at a 1 mg/ml concentration by probe sonication for 5 minutes. Then squamocin at a 1:3 w/w ratio, each from 50 mg/ml DMSO stock, was added and incubated overnight using a rotating shaker at RT to allow the adsorption of squamocin on ND surfaces. Finally, ND- squamocin complex was purified from free molecules by centrifugation at 14,000 rpm for 2 hours, and the pellet was washed with distilled water. The amount of free squamocin in the supernatant was analysed using a UV-VIS spectrophotometer. The compound loading efficiency (CLE) was calculated according to the following equation:

$$\text{CLE} = \frac{(\text{compound added initially} - \text{compound in the supernatant after centrifugation})}{(\text{compound added initially}) \times 100\%}$$

Nanodiamond particles were visualised using a transmission electron microscope (TEM), and the conjugation was confirmed and characterised using a scanning electron microscope (SEM) with 40.000x magnification.

## 2.5. Serum Collection

After the final day of treatments, the rats were sacrificed using ketamine anaesthesia (Tsai *et al.* 2016). The blood was taken from the left ventricle using a 26G injection needle and collected in a 5 ml microtube. The blood was left to stand for two hours to isolate the serum from the blood, then centrifuged at 1,000 rpm for 5 minutes, and the upper phase was then collected. The serum was stored at 4°C until further use.

## 2.6. Protein Isolation

The mammary tissue was isolated from the sacrificed rats and cleaned with buffer saline, and then it was put in a mortar containing liquid nitrogen and crushed using a pestle. The ground mammary tissue was filtered using a 200 mm filter, and the suspension was centrifuged at 2,000 rpm for 5 min. The pellets were collected, added with  $\text{NH}_4\text{Cl}$ , and centrifuged at 2,000 rpm for 5 min. The procedure was done repeatedly to obtain white pellets, and then the pellets were suspended in buffer saline and sonicated at 2 kHz for 20 sec (6 times) under ice-cold conditions. The supernatants were collected by centrifugation of homogenates at 2,500 rpm for 5 minutes and stored at -20°C for further use.

## 2.7. Determination of the Level of Malondialdehyde (MDA)

The MDA levels were measured using a Spectrophotometric Assay for Malondialdehyde (OxisResearch, #21044). The provided 10 mM TMOP stock solution was diluted with  $\text{ddH}_2\text{O}$  (1/500) to get 20  $\mu\text{l}$  of this solution. Final concentrations of 0; 0.5; 1.0; 2.0; 3.0; 4.0 to draw standard curve was obtained by mixing 0, 25, 50, 100, 150, 200  $\mu\text{l}$  of standard solution to 200, 175, 150, 125, 100, 75, 50, 25, 0  $\mu\text{l}$  of water as a total volume was 200  $\mu\text{l}$ . To each assay tube, 10  $\mu\text{l}$  of probucol and 200  $\mu\text{l}$  of the standard were added. Following this, 640  $\mu\text{l}$  of diluted R1 buffer (N-methyl-2-phenylindole in acetonitrile) was added to each tube and mixed by the vortex. Then, 150  $\mu\text{l}$  of diluted R2 buffer (concentrated hydrochloric acid) was added to each tube, mixed, and incubated for 60 min at 45°C. The clear supernatant was obtained by centrifugation at 10,000 rpm for 10 min. The absorbance was measured at 586 nm to get a standard curve against concentration for measuring MDA levels in the sample.

## 2.8. Enzyme-Linked Immunosorbent Assay (ELISA)

The levels of ERBB2 (Finetest, ER1910), p53 (Finetest, ER0394), PI3KCA (Finetest, ER0606), FOXC2 (Finetest, ER0479) and CA-15-3 (Finetest, ER0789) were determined by ELISA. Briefly, 50  $\mu\text{l}$  of standards (5000, 2500, 1000, 500, 250, 0 pg/ml) was added to each well and shaken gently. Then, 50  $\mu\text{l}$  of PBS with pH 7.0-7.2 was added into blank control, and 5  $\mu\text{l}$  of balance solution was added to 50  $\mu\text{l}$  of samples. In each well, 50  $\mu\text{l}$  of the conjugate was added except control. The plate was covered and incubated for 60 min at 37°C. The plate was washed with the diluted solution and air-dried. After that, substrate A and substrate B were added to each well, including control. The wells were covered and incubated for 15-20 min at 37°C. Fifty  $\mu\text{l}$  of stop solution was added to each well, including control and mixed. Optical density was measured at 450 nm by using ELISA-reader.

## 2.9. Hematoxylin Eosin (H.E.) Staining and Epithelial Thickness Measurement

Briefly, four-micrometre thick paraffin-embedded tissue blocks were sectioned onto slides and deparaffinised. The slides were then put in the oven overnight and deparaffinised. The slide was then stained with hematoxylin solution for 10 minutes, washed with running water, and incubated with acidic ethanol (1% HCl in 70% ethanol) for 5 seconds. After that, the slide was incubated with eosin staining for 5 minutes, washed, and incubated into alcohol series (ethanol 70% - ethanol absolute), followed by the series of xylol I and xylol II. The slides were mounted with entellan and observed using a microscope (Nikon, Japan). The epithelial thickness measurement was performed by using ImageJ software.

## 2.10. Immunohistochemistry Staining of Caspase-3 and Ki-67

Immunohistochemistry staining was performed according to the manufacturer's guidelines (Finetest, IHC0007). Briefly, four-micrometre thick paraffin-embedded tissue blocks were sectioned onto slides and deparaffinised. The slides were then put overnight in the oven and deparaffinised. The sections were quenched with 3% hydrogen peroxide in methanol for 30 min and blocked for one hour with blocking serum at 37°C. The slides were incubated with primary antibodies for Ki-67 (Invitrogen, MA5-14520) and Caspase-3 (Invitrogen, PA1-29157) overnight at 4°C, then washed, and using poly-HRP goat anti-rabbit IgG for secondary antibody at room

temperature for one hour. The colour was developed using 3,3'-diaminobenzidine tetrahydrochloride for 2 to 10 min, and the sections were then counterstained with hematoxylin. Images were acquired using a Nikon microscope (Japan) and digitally processed with the software for further analysis.

### 2.11. Statistical Analysis

Statistical analysis was performed by one-way analysis of variance (ANOVA) using PRISM software. The results were reported as the mean  $\pm$  standard deviation (SD), and a P-value of  $<0.05$  was considered statistically significant.

## 3. Results

### 3.1. Characterisation of Squamocin–nanodiamond Complex

TEM imaging showed that the nanodiamond particles' average size was expected to be less than 10 nm (Figure 1A). The conjugation of squamocin

onto nanodiamond was investigated by using SEM imaging. The result showed that the size of the complex was around 150–300 nm, indicating the success of the conjugation process (Figure 1B). In addition, the drug loading efficiency for each coating process was about 80–85%. Nanodiamond acts as the core of the nanoparticle complex. The carboxyl group on the nanodiamond surface binds with the amine group in mPEG amine. The squamocin was then binding to the ND-mPEG amine complex (Figure 1C).

### 3.2. The Thickness of the Mammary Ductal Epithelium and Serum Level of CA-15-3

To investigate the growth inhibition effect of NDSQ on rats-induced breast cancer, we measured the thickness of mammary ductal epithelium following HE staining of the tissue (Figure 2A). The thickness of mammary ductal epithelium in the normal control group was  $7.024 \pm 0.579$  mm, and it was significantly increased compared to the negative control group ( $30.243 \pm 7.124$  mm). The treatment

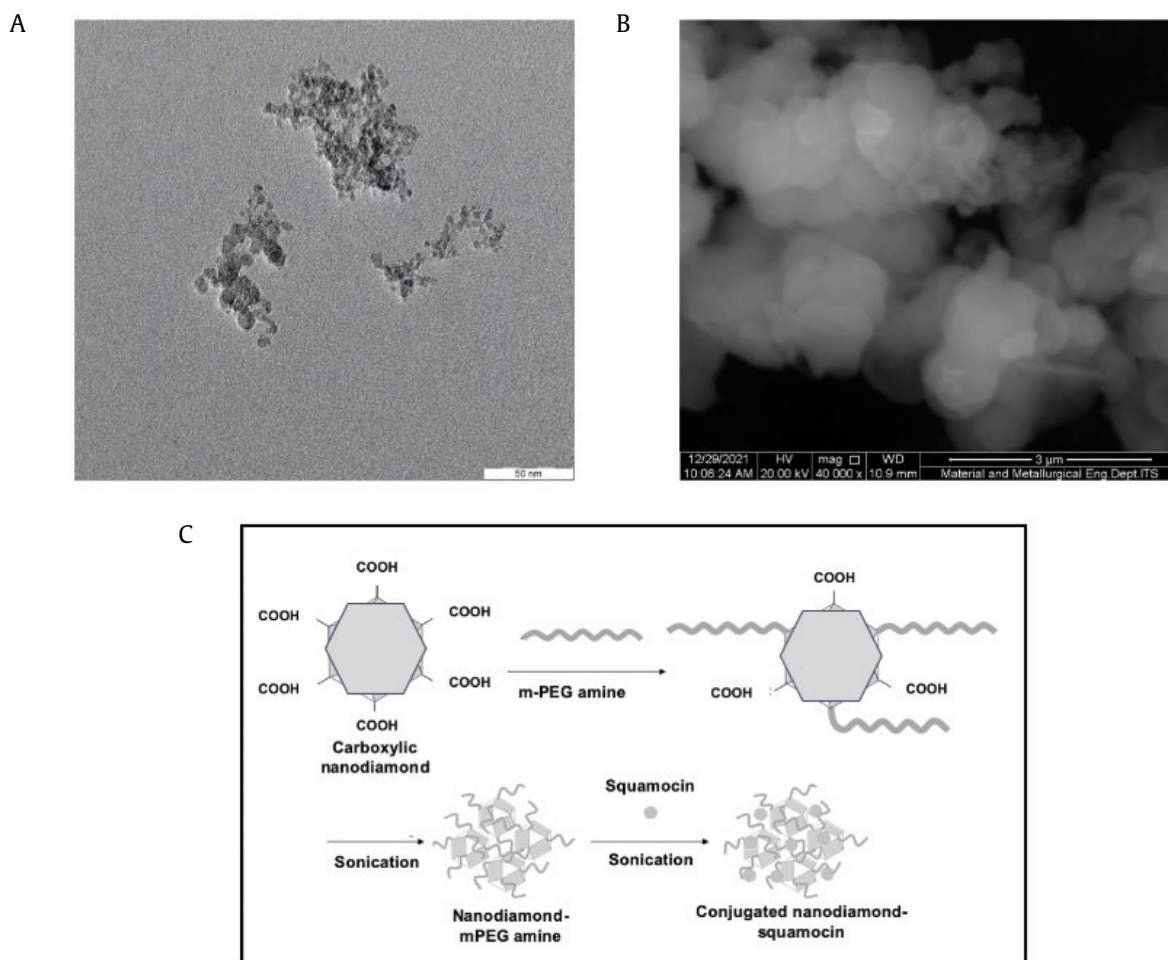


Figure 1. (A) Imaging of nanodiamond particle by using TEM with 100,000x magnification, (B) imaging of squamocin-nanodiamond complex by using SEM (magnification 40,000x), (C) interaction scheme between ND, mPEG amine, and squamocin

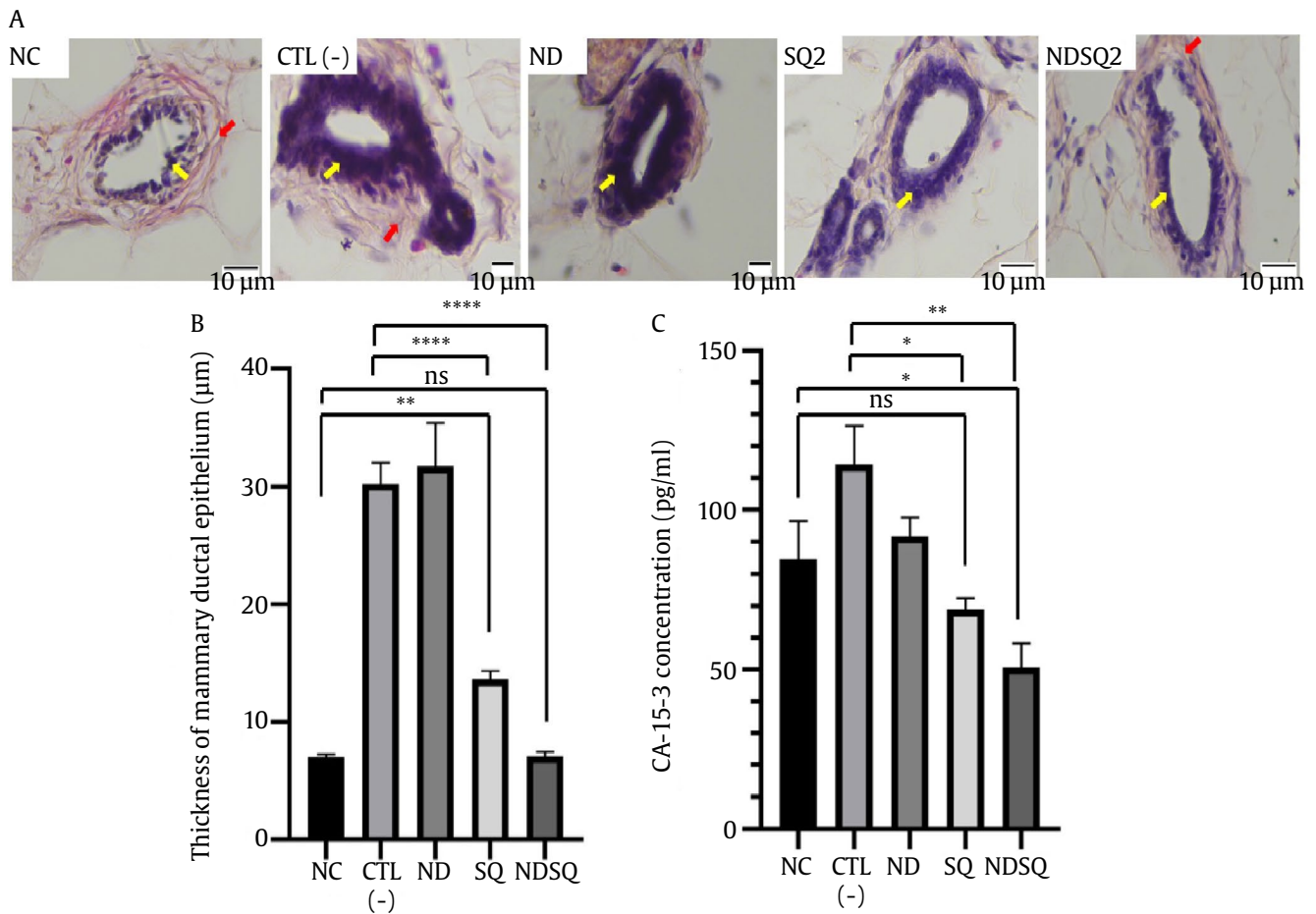


Figure 2. The effect of nanodiamond coupled with squamocin on the mammary ductal epithelium and serum level of CA-15-3 in rat model following treatment with 1.5 mg/kg body weight of NDSQ for 5 weeks. (A) HE was staining the mammary ductal epithelium, (B) quantification of the thickness of the mammary ductal epithelium, (C) serum level of CA-15-3. NC: normal control group, CTL(-): negative control group, ND: nanodiamond group, SQ: squamocin group; NDSQ: squamocin coupled with nanodiamond group. Each bar represents mean  $\pm$  SD

with SQ can significantly reduce the thickness of mammary ductal epithelium to  $13.644 \pm 1.184$  mm, and treatment with NDSQ can reduce the thickness even further ( $7.076 \pm 0.748$  mm). We found that both SQ and NDSQ can significantly reduce the thickness of the mammary ductal epithelium, but only NDSQ can reduce the thickness close to the average epithelium thickness (Figure 2B).

We also examined the serum level of CA-15-3 protein, a marker for breast cancer metastasis. We found that the CA-15-3 level in serum was significantly higher in the negative control group ( $114.3 \pm 12.06$  pg/ml) than in the normal control group ( $84.74 \pm 11.80$  pg/ml), and it was significantly reduced in the SQ ( $68.81 \pm 3.58$  pg/ml) and NDSQ ( $50.75 \pm 7.54$  pg/ml) groups. The serum level of CA-15-3 in the SQ and NDSQ group was not significantly different compared to the normal control, suggesting that

both SQ and NDSQ can reduce CA-15-3 levels similar to normal levels (Figure 2C).

### 3.3. Caspase-3 and Ki-67 Expression

The percentage of cells with positive Caspase-3 staining was significantly increased in the SQ group ( $5.28 \pm 0.91$ ) and NDSQ group ( $6.868 \pm 0.83$ ) compared to the negative control ( $1.67 \pm 0.21$ ). The SQ group was significantly different from the normal control group ( $7.29 \pm 1.00$ ), but NDSQ showed no significant difference. In contrast, the percentage of cells with positive Ki-67 staining was significantly reduced in the SQ group ( $8.99 \pm 0.94$ ) and NDSQ group ( $6.50 \pm 0.97$ ) compared to the negative control ( $14.40 \pm 1.75$ ). Meanwhile, SQ and NDSQ groups showed no difference compared to the normal control group ( $6.03 \pm 0.71$ ) (Figure 3A-C).

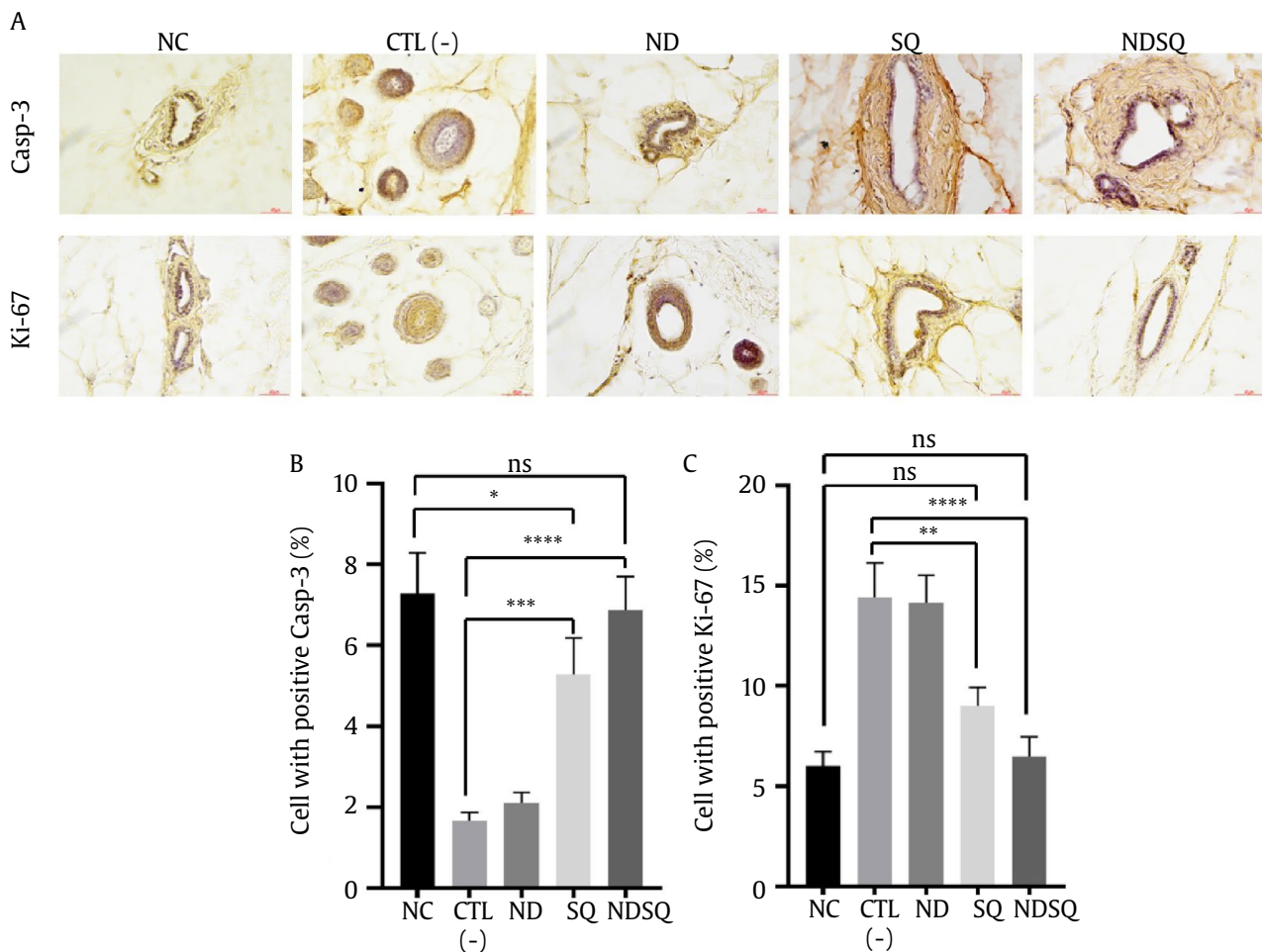


Figure 3. Cells with positive Caspase-3 and Ki-67 staining following treatment with 1.5 mg/kg body weight of NDSQ for 5 weeks. (A) Caspase-3 and Ki-67 expression by immunohistochemistry staining, (B) quantifying cells with positive Caspase-3 expression, and (C) quantifying cells with positive Ki-67 expression. NC: normal control group, CTL (-): negative control group, ND: nanodiamond group, SQ: squamocin group, NDSQ: squamocin coupled with nanodiamond group. Each bar represents mean  $\pm$  SD

### 3.4. Serum MDA Level

To investigate the antioxidant activity of squamocin, we measured the MDA level in serum. The MDA levels in the SQ group ( $1129 \pm 155$  pmol/ml) were not significantly reduced compared to the negative control group ( $1561 \pm 285$  pmol/ml). However, the MDA levels in the NDSQ group ( $416 \pm 184$  pmol/ml) were significantly lower than in the negative control group (Figure 4).

### 3.5. ERBB2, PI3KCA, p53 and FOXC2 Expression

To analyse the signalling pathway affected by squamocin, we performed protein expression analysis by using ELISA. We first examined the ErbB2 level as one of the upstream molecules of PI3K. The level of ERBB2 and FOXC2 was not significantly different in each group. We then examined the protein level of PI3KCA/P110a (subunits of PI3K) expression. The

result shows that PI3KCA expression significantly increased in the negative control group compared to the normal control group. In the SQ group, the level of PI3KCA showed a similar level to the negative control group. However, treatment with NDSQ could significantly reduce the PI3KCA expression compared to the negative control. In addition, we also analysed the level of one downstream target of the PI3K/Akt pathway, tumor suppressor protein p53. The level of p53 significantly increased in both SQ and NDSQ groups compared to the negative control (Table 1).

## 4. Discussion

Cancer remains one of the leading causes of death worldwide despite the considerable effort and resources in cancer therapy. Cancer is abnormal cell proliferation and the failure of cells to die due

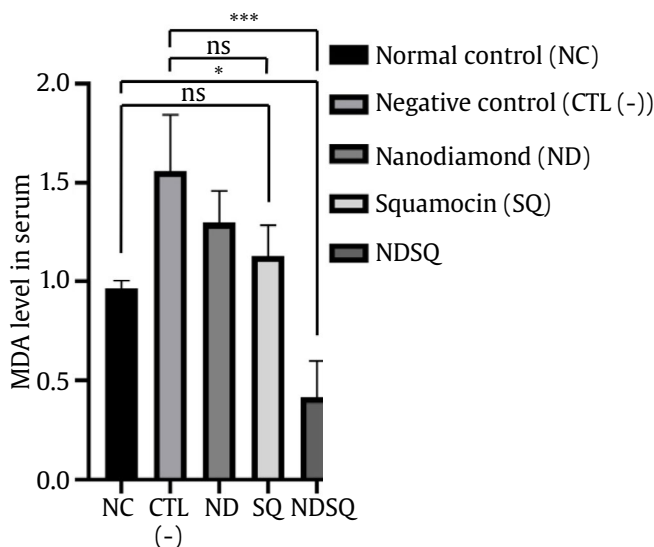


Figure 4. The serum level of MDA in the rat model was treated with 1.5 mg/kg body weight of nanodiamond coupled with squamocin for 5 weeks. NC: normal control group, CTL(-): negative control group, ND: nanodiamond group, SQ: squamocin group, NDSQ: squamocin coupled with nanodiamond group. Each bar represents mean ± SD

Table 1. The protein level of ERBB2, PI3KCA, p53 and FOXC2 after treatment with squamocin coupled with nanodiamond

Group	Protein			
	ERBB2	PI3KCA	P53	FOXC2
NC	0.44±0.02 <sup>a</sup>	68.98±22.19 <sup>a</sup>	1186±201.58 <sup>a</sup>	0.080±0.001 <sup>a</sup>
CTL(-)	0.41±0.01 <sup>a</sup>	130.4±15.36 <sup>b</sup>	138.4±8.81 <sup>b</sup>	0.084±0.001 <sup>a</sup>
ND	0.42±0.01 <sup>a</sup>	134.6±39.88 <sup>b</sup>	77.24±2.8 <sup>b</sup>	0.084±0.005 <sup>a</sup>
SQ	0.44±0.02 <sup>a</sup>	135.1±3.40 <sup>b</sup>	937.7±12.24 <sup>a</sup>	0.084±0.001 <sup>a</sup>
NDSQ	0.43±0.002 <sup>a</sup>	41.93±14.85 <sup>a</sup>	823.6±18.61 <sup>a</sup>	0.081±0.002 <sup>a</sup>

NC: normal control group, CTL(-): negative control group, ND: nanodiamond group, SQ: squamocin group, NDSQ: squamocin coupled with nanodiamond group. The different numbers showed statistically significant

to the accumulation of gene mutations. In this study, the anti-cancer activity of squamocin was shown by the reduction of the thickness of the mammary gland epithelium. This reduction was accompanied by an increase in apoptosis and a reduction in cell proliferation (Figures 2 and 3). The resistance to apoptosis is a hallmark of cancer (Wang *et al.* 2013). In this study, the apoptosis rate was significantly reduced compared to the normal control group in the negative control group. Treatment with SQ and NDSQ significantly increased the percentage of apoptotic cells. However, the percentage of apoptotic cells in the NDSQ group was higher compared to the SQ group (Figure 3). The results suggest nanodiamond's efficiency as

a carrier to bring squamocin effectively to the tumor microenvironment. The result of this study was supported by a previous study that reported the effect of squamocin in bladder T24 cancer cells. Squamocin induces apoptotic through the expression of the proapoptotic genes Bax and Bad, resulting in the cleavage of PARP and the enhanced activity of Caspase-3 (Yuan *et al.* 2006).

The increase of proliferating cells rather than the speed of cell division is responsible for cancer growth. The ratio of proliferating cells in the total pool of cells was called the growth fraction (Wang *et al.* 2013). The Ki-67 staining usually labels the proliferating cells. In this study, the number of proliferating cells increased significantly in the negative control group compared to the normal control group (Figure 3). Treatment with SQ and NDSQ significantly reduced the number of proliferating cells, suggesting the growth inhibition activity of squamocin. We also examined the serum level of CA-15-3 as a marker to monitor metastatic breast cancer. Here we showed that the CA-15-3 level was significantly reduced in SQ and NDSQ group compared to the negative control group, suggesting its ability to prevent metastasis of breast cancer cells. Serum CA-15-3 monitors metastatic breast cancer patients undergoing treatment and preclinical tumor recurrence detection (Hashim 2013; Keshaviah *et al.* 2007).

The complex physiological features of the tumor microenvironment include hypoxia resulting from overconsumption of oxygen due to rapid tumor development (Jaskiewicz *et al.* 2022). About 50–60% of solid tumors exhibit decreased oxygen levels (Vaupel and Mayer 2007). Hypoxia is associated with cancer cell growth, metastasis, and resistance to therapies. In addition, hypoxia also stimulates the production of mitochondrial ROS, and tumor cells produce a higher level of ROS than normal tissue (Costa *et al.* 2014; Jezierska-Drutel *et al.* 2013). Increased levels of ROS also observed in many cancer cell lines (Szatrowski and Nathan 1991).

ROS plays a vital role in carcinogenesis and affects multiple biological processes, such as cell proliferation, differentiation, genomic instability, inflammation, cell survival, resistance to apoptosis, and metabolic reprogramming. ROS can lead to lipid peroxidation, which often is monitored by measuring the MDA level. Recent studies reported that plasma MDA levels in breast, lung, and bladder cancer patients were significantly higher than in control (Gonenc *et al.* 2001; Lepara *et al.* 2020). Serum levels of MDA play an essential role as a biomarker in diagnosing bladder cancer and

monitoring its progression. Serum MDA level in patients with high grades of bladder cancer was significantly higher than the serum MDA level in patients with a low grade of bladder cancer (Lepara *et al.* 2020). MDA is one of the best-investigated products of lipid peroxidation. It is presumed that MDA acts as a tumor promoter and a co-carcinogenic agent because of its high cytotoxicity and inhibitory action on antioxidant enzymes. The MDA serum level reflects free-radical cell damage (Seven *et al.* 1999). In this study, the MDA levels in the SQ group were not significantly reduced compared to the negative control group. However, the MDA levels in the NDSQ group were significantly lower than the negative control group, suggesting the effectivity of nanodiamond as a carrier of squamocin to increase its antioxidant property.

ROS-sensitive signalling pathways are often elevated in many types of cancers. Reactive oxygen species can act as second messengers in cellular signalling. Hydrogen peroxide ( $H_2O_2$ ) regulates protein activity through reversible oxidation of its targets, including protein and receptor tyrosine kinase (Chiarugi and Fiaschi 2007; Storz 2005). ROS generation during estrogen metabolism or other potential mammary carcinogens activated the PI3K/Akt signalling pathway (Burdick *et al.* 2003; Park *et al.* 2009). Inhibition of ROS in the human pancreatic tumor cell line reduced the level of active phosphorylated Akt, thus, inducing apoptosis (Mochizuki *et al.* 2006). A signalling cascade including PI3K tightly controls Akt activity. In this study, we showed that the protein level of PI3KCA was significantly increased in the negative control group compared to the normal control, suggesting the critical role of this protein during carcinogenesis. The increase in PI3KCA expression was not correlated with ERBB2 protein expression. ERBB2 expression in all treatment groups was not significantly different, suggesting that another upstream receptor mediated the modulation of PI3KCA expression. In the SQ group, the level of PI3KCA showed a similar level to the negative control group. However, treatment with NDSQ could significantly reduce the PI3KCA expression compared to the negative control (Table 1). This result suggests nanodiamond's effectivity as a carrier to increase squamocin activity. In addition, we also analysed the level of one downstream target of the PI3K/Akt pathway, tumor suppressor protein p53. The protein level of p53 was significantly lower in the negative control than in the normal control group, suggesting its essential role as a tumor suppressor protein. Treatment with SQ and NDSQ could significantly increase the p53 levels compared to the negative control.

The level of p53 in the SQ group significantly increased compared to the negative control group while the PI3KCA level was still high, suggesting the regulation of p53 expression is not solely depends on PI3KCA expression. Protein p53 is a tumor suppressor protein involved in the apoptotic process. The primary function of p53 is to prevent the replication of cells with DNA damage. Therefore, p53 is inactive, and the damaged cells continue to grow and replicate DNA mutations (Okada and Mak 2004).

In conclusions, a dynamic and complex tumor microenvironment promotes tumor progression and is a promising target for anti-cancer treatment. A high level of ROS in the tumor microenvironment activates several signalling cascades, including PI3K activity. In this study, we showed that the growth inhibition activity of squamocin coupled with nanodiamond in rat-induced breast cancer was mediated by reduced proliferating cells and apoptosis induction in breast cancer cells. Squamocin coupled with nanodiamond also reduced MDA level and PI3KCA expression, followed by increased p53 expression. The level of CA-15-3 as a metastasis marker of breast cancer was also significantly reduced in the group treated with squamocin and squamocin coupled with nanodiamond, which later reduced its expression further. We are the first to use nanodiamond as a carrier of squamocin to increase its availability and anti-cancer activity in rat-induced breast cancer.

### Conflict of Interest

The authors declare that there is no conflict of interest regarding the publication of this paper.

### Acknowledgements

This work was funded by Hibah Riset Mandat Dosen Muda, Universitas Airlangga, Indonesia (grant number: 390/UN3.14/PT/2020).

### References

- Bahrami, A., Hassanian, S.M., 2018. The therapeutic potential of targeting tumor microenvironment in breast cancer: rational strategies and recent progress. *J. Cell. Biochem.* 1, 111e22. <https://doi.org/10.1002/jcb.26183>
- Balkwill, F.R., Capasso, M., Hagemann, T., 2012. The tumor microenvironment at a glance. *J. Cell. Sci.* 23, 5591e6. <https://doi.org/10.1242/jcs.116392>
- Burdick, A.D., Davis, 2<sup>nd</sup> J.W., Liu, K.J., Hudson, L.G., Shi, H., Monske, M.L., 2003. Benzo(a)pyrene quinones increase cell proliferation, generate reactive oxygen species, and transactivate the epidermal growth factor receptor in breast epithelial cells. *Cancer. Res.* 63, 7825–7833.

- Cheng, Y.T., Yang, C.C., Shyur, L.F., 2016. Phytomedicine-modulating oxidative stress and the tumor microenvironment for cancer therapy. *Pharmacol Res.* 114, 128e43. <https://doi.org/10.1016/j.phrs.2016.10.022>
- Chiarugi, P., Fiaschi, T., 2007. Redox signalling in anchorage-dependent cell growth. *Cell Signal.* 19, 672–682. <https://doi.org/10.1016/j.cellsig.2006.11.009>
- Costa, A., Scholer-Dahirel, A., Mechta-Grigoriou, F., 2014. The role of reactive oxygen species and metabolism on cancer cells and their microenvironment. *Semin. Cancer Biol.* 25, 23–32. <https://doi.org/10.1016/j.semcancer.2013.12.007>
- Danhier, F., 2016. To exploit the tumor microenvironment: since the EPR effect fails in the clinic, what is the future of nanomedicine?. *J. Control. Release.* 244, 108–121. <https://doi.org/10.1016/j.jconrel.2016.11.015>
- Ghaferi, Z., Zahra, W., Akbarzadeh, A., Ebrahimi Shahmabadi, H., Alavi, S.E., 2022. Enhancing the efficacy of albendazole for liver cancer treatment using mesoporous silica nanoparticles: an *in vitro* study. *EXCLI Journal.* 21, 236–249. <https://doi.org/10.21203/rs.3.rs-294729/v1>
- Gönenç A., Ozkan, Y., Torun, M., Simşek, B., 2001. Plasma malondialdehyde (MDA) levels in breast and lung cancer patients. *J. Clin. Pharm. Ther.* 26, 141–144. <https://doi.org/10.1046/j.1365-2710.2001.00334.x>
- Hashim, Z.M., 2013. The significance of CA 15-3 in breast cancer patients and its relationship to HER-2 receptor status. *International Journal of Immunopathology and Pharmacology.* 27, 45–51. <https://doi.org/10.1177/039463201402700107>
- Jaskiewicz, M., Moszynska, A., Serocki, M., Krolczewski, J., Bartoszewska, S., Collawn, J.F., Bartoszewski, R., 2022. Hypoxia-inducible factor (HIF)3 $\alpha$ 2 serves as an endothelial cell fate executor during chronic hypoxia. *EXCLI Journal.* 21, 454–469.
- Jeziarska-Drutel, A., Rosenzweig, S.A., Neumann, C.A., 2013. Role of oxidative stress and the microenvironment in breast cancer development and progression. *Adv. Cancer Res.* 119, 107–125. <https://doi.org/10.1016/B978-0-12-407190-2.00003-4>
- Keshaviah, A., Dellapasqua, S., Rotmensz, N., Lindtner, J., Crivellari, D., Collins, J., 2007. CA15-3 and alkaline phosphatase as predictors for breast cancer recurrence: a combined analysis of seven International Breast Cancer Study Group trials. *Annals of Oncology.* 18, 701–708. <https://doi.org/10.1093/annonc/mdl492>
- Lepara, Z., Lepara, O., Fajkic, A., Rebic, D., Alic, J., Spahovic, H., 2020. Serum malondialdehyde (MDA) level as a potential biomarker of cancer progression for patients with bladder cancer. *Rom. J. Intern. Med.* 58, 146–152. <https://doi.org/10.2478/rjim-2020-0008>
- Li, J., Gu, B., Meng, Q., Yan, Z., Gao, H., Chen, X., 2011. The use of myristic acid as a ligand of polyethylenimine/DNA nanoparticles for targeted gene therapy of glioblastoma. *Nanotechnology.* 43, 435101e9. <https://doi.org/10.1088/0957-4484/22/43/435101>
- Li, J., Burgess, D.J., 2020. Nanomedicine-based drug delivery towards tumor biological and immunological microenvironment. *Acta Pharmaceutica Sinica B.* 10, 2110e2124. <https://doi.org/10.1016/j.apsb.2020.05.008>
- Liaw, C.C., Wu, T.Y., Chang, F.R., Wu, Y.C., 2010. Historic perspectives on *Annonaceous acetogenins* from the chemical bench to preclinical trials. *Planta Medica.* 76, 1390–1404. <https://doi.org/10.1055/s-0030-1250006>
- Lu, M.C., Yang, S.H., Hwang, S.L., Lu, Y.J., Lin, Y.H., Wang, S.R., 2006. Induction of G2/M phase arrest by squamocin in chronic myeloid leukemia (K562) cells. *Life Sciences.* 78, 2378–2383. <https://doi.org/10.1016/j.lfs.2005.09.048>
- Miao, Y., Xu, X., Yuan, F., Shi, Y., Chen, Y., Chen, J., 2016. Four cytotoxic annonaceous acetogenins from the seeds of *Annona squamosa*. *Natural Product Research.* 30, 1273–1279. <https://doi.org/10.1080/14786419.2015.1055490>
- Mochizuki, T., Furuta, S., Mitsushita, J., Shang, W.H., Ito, M., Yokoo, Y., 2006. Inhibition of NADPH oxidase 4 activates apoptosis via the AKT/apoptosis signal-regulating kinase 1 pathway in pancreatic cancer PANC-1 cells. *Oncogene.* 25, 3699–3707. <https://doi.org/10.1038/sj.onc.1209406>
- Okada, H., Mak, T.W., 2004. Pathways of apoptotic and non-apoptotic death in tumour cells. *Nat. Rev. Cancer.* 4, 592–603. <https://doi.org/10.1038/nrc1412>
- Paplomata, E., O'Regan, R., 2014. The PI3K/AKT/mTOR pathway in breast cancer: targets, trials and biomarkers. *Ther. Adv. Med. Oncol.* 6, 154–166. <https://doi.org/10.1177/1758834014530023>
- Park, S.A., Na, H.K., Kim, E.H., Cha, Y.N., Surh, Y.J., 2009. 4-hydroxyestradiol induces anchorage-independent growth of human mammary epithelial cells via activation of I $\kappa$ B kinase: potential role of reactive oxygen species. *Cancer Res.* 69, 2416–2424. <https://doi.org/10.1158/0008-5472.CAN-08-2177>
- Purtov, K.V., Petunin, A.I., Burov, A.E., Puzyr, A.P., Bondar, V.S., 2010. Nanodiamonds as carriers for address delivery of biologically active substances. *Nanoscale Research Letters.* 5, 631–636. <https://doi.org/10.1007/s11671-010-9526-0>
- Seven, A., Civelek, S., Inci, E., Korkut, N., Burçak, G., 1999. Evaluation of oxidative stress parameters in blood of patients with laryngeal carcinoma. *Clin. Biochem. J.* 32, 69–73. [https://doi.org/10.1016/S0009-9120\(99\)00022-3](https://doi.org/10.1016/S0009-9120(99)00022-3)
- Storz, P., 2005. Reactive oxygen species in tumor progression. *Front. Biosci.* 10, 1881–1896. <https://doi.org/10.2741/1667>
- Szatrowski, T.P., Nathan, C.F., 1991. Production of large amounts of hydrogen peroxide by human tumor cells. *Cancer Res.* 51, 794–798.
- Tsai, F.F., Fan, S.Z., Lin, Y.S., Huang, N.E., Yeh, J.R., 2016. Investigating power density and the degree of nonlinearity in intrinsic components of anesthesia EEG by the hilbert-huang transform: an example using ketamine and alfentanil. *PLOS ONE.* 11, e0168108. <https://doi.org/10.1371/journal.pone.0168108>
- Vaupel, P., Mayer, A., 2007. Hypoxia in cancer: significance and impact on clinical outcome. *Cancer Metastasis Rev.* 2, 225e39. <https://doi.org/10.1007/s10555-007-9055-1>
- Velazquez Berumen, A., Jimenez Moyao, G., Rodriguez, N.M., Ilbawi, A.M., Migliore, A., Shulman, L.N., 2018. Defining priority medical devices for cancer management: a WHO initiative. *Lancet Oncol.* 19, 709–719. [https://doi.org/10.1016/S1470-2045\(18\)30658-2](https://doi.org/10.1016/S1470-2045(18)30658-2)
- Wang, R.A., Li, Q.L., Li, Z.S., Zheng, P.J., Zhang, H.Z., Huang, X.F., Chi, S.M., Yang, A.G., Cui, R., 2013. Apoptosis drives cancer cells proliferate and metastasise. *J. Cell. Mol. Med.* 17, 205–211. <https://doi.org/10.1111/j.1582-4934.2012.01663.x>
- Wei, S., Li, L., Du, X., Li, Y., 2019. Off-On nanodiamond drug platform for targeted cancer imaging and therapy. *Journal of Materials Chemistry B.* 7, 3390–3402. <https://doi.org/10.1039/C9TB00447E>
- Yuan S.S., Chang, H.L., Chen H.W., Kuo F.C.H., Liaw, C.H.C.H., Su, J.H., 2006. Selective cytotoxicity of squamocin on T24 bladder cancer cells at the S-phase via a Bax-, Bad- and caspase-3-related pathways. *Life Sci.* 78, 869–874. <https://doi.org/10.1016/j.lfs.2005.05.068>